Volume 59
Number 78
7 October 2023
Pages 11597–11742

ChemComm

Chemical Communications

rsc.li/chemcomm

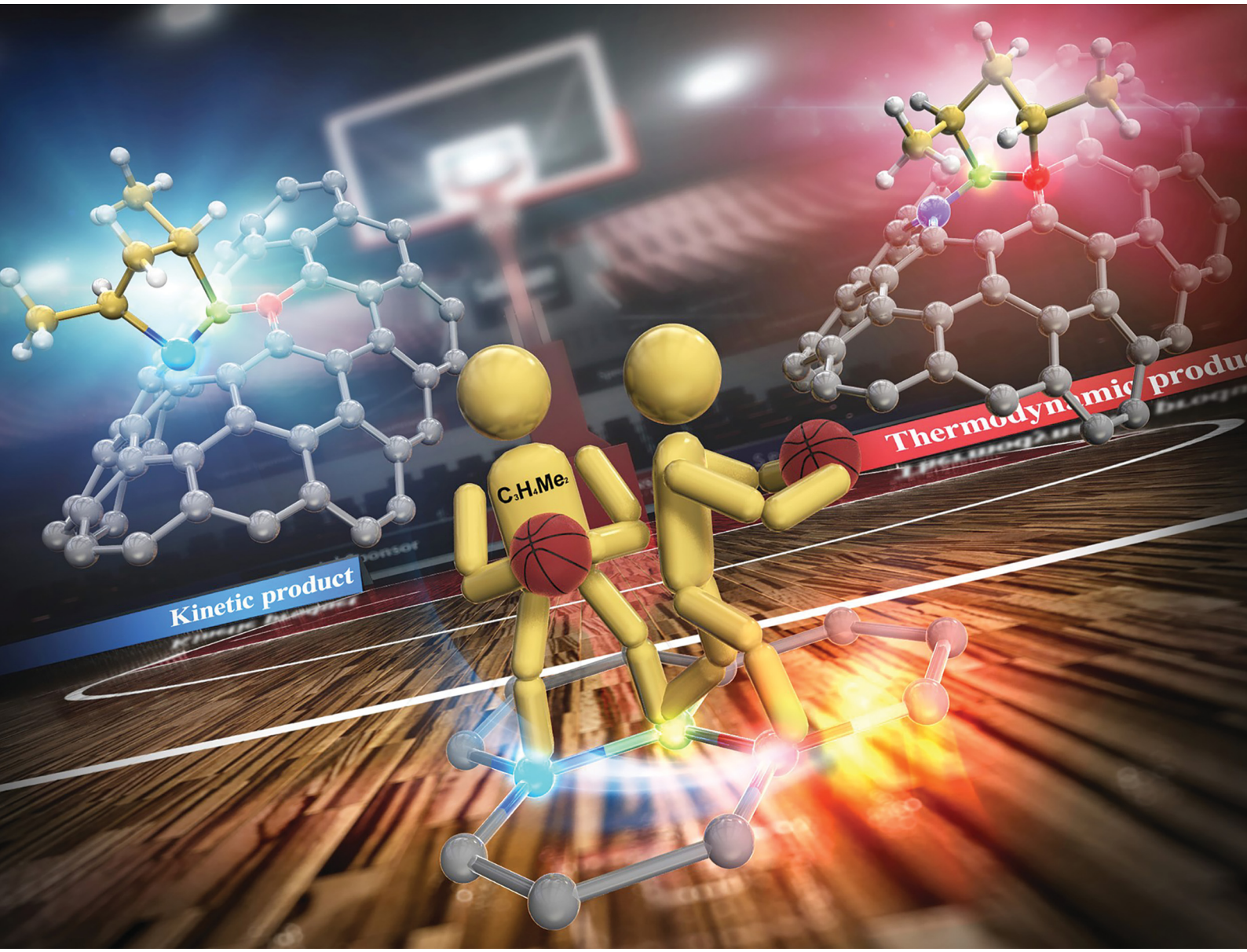

ISSN 1359-7345

ROYAL SOCIETY OF CHEMISTRY

COMMUNICATION

Yutaka Maeda, Pei Zhao, Masahiro Ehara *et al.*
Control of functionalized single-walled carbon nanotube photoluminescence *via* competition between thermal rearrangement and elimination

ChemComm

COMMUNICATION

View Article Online
View Journal | View Issue

Cite this: *Chem. Commun.*, 2023, 59, 11648

Received 21st June 2023,
Accepted 22nd August 2023

DOI: 10.1039/d3cc02965d

rsc.li/chemcomm

Control of functionalized single-walled carbon nanotube photoluminescence *via* competition between thermal rearrangement and elimination†

Yutaka Maeda, *[a] Rina Morooka,[a] Pei Zhao, *[b] Michio Yamada [a] and Masahiro Ehara *[b]

We conducted the chiral separation of functionalized single-walled carbon nanotubes (SWNTs) with dibromopropane derivatives. Depending on their chirality and diameter, the thermal treatment of functionalized SWNTs leads to a shift in the emission radiation to longer wavelengths owing to rearrangement reaction in competition with elimination reaction.

Single-walled carbon nanotubes (SWNTs) are cylindrical carbon nanomaterials that have attracted special attention owing to their unique electronic and optical properties.[1,2] Various chemical functionalization methods have been developed, and unique chemical reactivity depending on the electronic structure and diameter has been reported.[3–7] The functionalization degree of SWNTs significantly impacts their intrinsic properties because excessive functionalization disturbs the π-electron system of SWNTs.[8,9] The functionalization degree of SWNTs can be estimated by spectroscopic analysis, the decrease of their intrinsic absorption and photoluminescence (PL) peaks, and the increase of the D- to G-band intensity ratio (D/G) in the Raman spectra.[7,8] SWNTs with smaller diameters were shown to have higher reactivity because of their higher strain energy, and their adducts are thermodynamically more stable than those of SWNTs with larger diameters.[10,11]

The functionalization of SWNTs was recently reported to reduce the band gap locally at the addition site, as revealed by PL measurements at an appropriate functionalization degree.[12,13] New PL peaks in the near-infrared (NIR) region were emerged in high quantum yield by functionalization, enabling excitation at the E_{11} energies and thus facilitating the application of SWNTs as an NIR light source in fields such as bioimaging and sensing.[14] Systematic theoretical calculations using model compounds revealed that the binding configuration of addenda is an important factor for the local band gap energy.[15–17] In other words, it is expected that the PL wavelength of SWNT adducts provides insight into their local structure. Previously, we reported that functionalization of (6,5) SWNTs with 1,*n*-dibromoalkanes, $Br(CH_2)_nBr$ (n = 3–5), emerged a new PL peak at 1215–1231 nm depending on the alkyl lengths; the PL intensity was affected by the functionalization degree, which was modified through the partial elimination of the addenda *via* thermal treatment.[18] In contrast, the PL wavelength of (6,5) SWNTs functionalized using 2,4-dibromopentane (mixture of stereoisomers) changed from 1219 to 1268 nm after the thermal treatment, indicating thermal rearrangement, *i.e.*, changing of binding configuration (Scheme 1 and Fig. S1, ESI†).[19] The combination of functionalization and thermal treatment extended the PL wavelength range of (6,5) SWNTs[19–22] to 1268 nm, reaching the original-band in the optical communication wavelength bands. He *et al.*, demonstrated that SWNTs with PL controlled by arylation produce room-temperature single-photon emission in the telecom band. The development of new methods for effectively and selectively generating new PL peaks in the telecom band has a high potential for applications.[23]

As previously mentioned, theoretical calculations indicated that the PL wavelength of functionalized SWNTs isomers is governed by the binding configuration of the addenda. Therefore, the PL wavelength after functionalization can be a probe for the binding configuration of the functionalized SWNTs. Herein, we investigated how the thermal treatment and chiral separation of SWNTs-$C_3H_4Me_2$ can expand the excitation and emission wavelengths of SWNTs. The results showed that the emission of various chiral semiconducting SWNTs can be

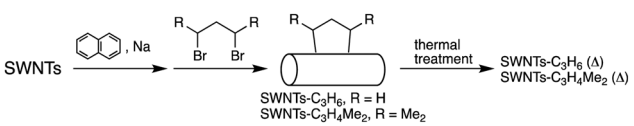

Scheme 1 Functionalization of SWNTs and subsequent thermal treatment.

[a] *Department of Chemistry, Tokyo Gakugei University, Tokyo 184-8501, Japan. E-mail: ymaeda@u-gakugei.ac.jp*
[b] *Research Center for Computational Science, Institute for Molecular Science, Okazaki 444-8585, Japan. E-mail: pei@ims.ac.jp, ehara@ims.ac.jp*

† Electronic supplementary information (ESI) available. See DOI: https://doi.org/10.1039/d3cc02965d

shifted to longer wavelengths by the thermal rearrangement competing with the elimination reaction, in a diameter dependent manner.

Fig. 1 and 2 depict the PL spectra of the separated SWNTs-C_3H_6 and SWNTs-$C_3H_4Me_2$ before and after thermal treatment. For a detailed explanation of separation of SWNTs, see ESI† (Fig. S2–S16).[24–29] The characteristic PL peaks were assigned based on the relationship between the excitation wavelengths and the E_{22} and E_{11} energies for each chiral SWNTs (Table 1).[27] The chiral index assignment for each PL peak is shown in PL mapping (Fig. S17–S23, ESI†). A single new PL peak was observed selectively for each chiral SWNTs-C_3H_6 adduct. In (6,4), (7,3), and (6,5) SWNTs-C_3H_6, no significant change in PL wavelengths was observed after thermal treatment at 400 °C. In contrast, in (8,3), (7,5), and (8,4) SWNTs, the intensity of E_{11} PL peaks at respectively 957, 1035, and 1122 nm, respectively, increased after thermal treatment with a decrease of the PL peaks emerged by functionalization (Fig. 1d–f). The results suggest that the thermal treatment resulted in an elimination reaction. In addition, (8,3) and (7,5) SWNTs-C_3H_6 (400 °C) exhibited new PL peaks at 1249 and 1266 nm, respectively. Therefore, the thermal treatment of SWNTs-C_3H_6 is effective in diameter-selectively controlling the PL intensities emerged after functionalization. Moreover, the emergence of new PL peaks in (8,3) and (7,5) SWNTs-C_3H_6 (400 °C), for which (mod(n-m, 3) = 2), indicates competing rearrangement and elimination reactions.

The separated (7,3), (6,5), and (8,4) SWNTs-$C_3H_4Me_2$, for which (mod(n-m, 3) = 1), each exhibited a single new PL peak at similar wavelengths to those of SWNTs-C_3H_6 (Fig. 2). After thermal treatment at 300 °C for 6 h, PL peaks at 1317 and 1268 nm were observed in (7,3) and (6,5) SWNTs-$C_3H_4Me_2$ (300 °C, 6 h), respectively, accompanied by an increase of the intrinsic E_{11} PL peak. In contrast, after thermal treatment at

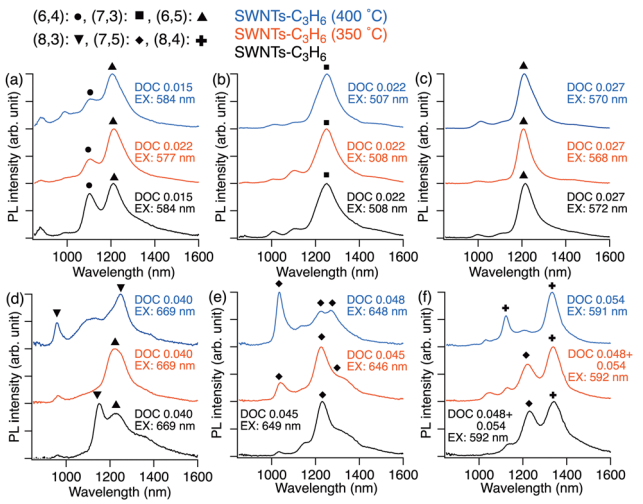

Fig. 1 PL spectra of separated SWNTs-C_3H_6 before and after thermal treatment dispersed in D_2O solution containing 1 wt% SC. Black line: SWNTs-C_3H_6. Red line: SWNTs-C_3H_6 (350 °C). Blue line: SWNTs-C_3H_6 (400 °C). Excitation wavelengths and peak assignment are shown in each spectrum.

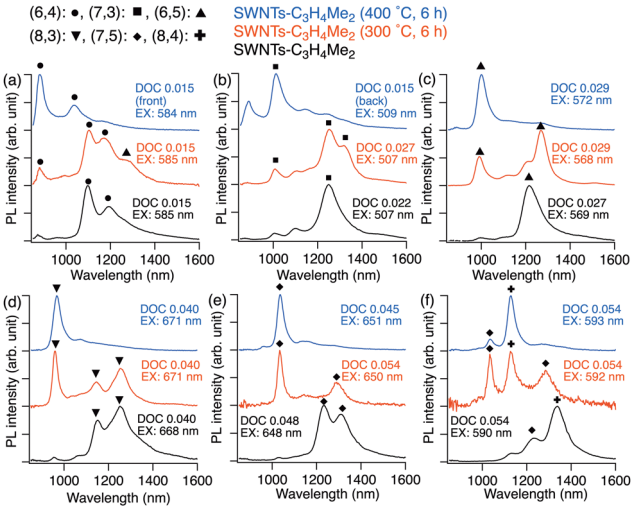

Fig. 2 PL spectra of separated SWNTs-$C_3H_4Me_2$ before and after thermal treatment dispersed in D_2O solution containing 1 wt% SC. Black line: SWNTs-$C_3H_4Me_2$. Red line: SWNTs-$C_3H_4Me_2$ (300 °C, 6 h). Blue line: SWNTs- $C_3H_4Me_2$ (400 °C, 6 h). Excitation wavelengths and peak assignment are shown in each spectrum.

Table 1 PL wavelengths of separated SWNTs-$C_3H_4Me_2$ before and after thermal treatment

	(6,4)	(7,3)	(6,5)	(8,3)	(7,5)	(8,4)
SWNTs-$C_3H_4Me_2$	1098	1249	1213	1151	1234	1337
	1192			1251	1310	
SWNTs-$C_3H_4Me_2$ (200 °C, 6 h)	1104	1252	1210	1157	1237	1337
	1190			1252	1299	
SWNTs-$C_3H_4Me_2$ (300 °C, 6 h)	1104	1252	1268	1146	1298	
	1174	1317		1255		
SWNTs-$C_3H_4Me_2$ (400 °C)	1102	1246	1269	1130	1290	
	1157	1323		1251		
SWNTs-$C_3H_4Me_2$ (400 °C, 6 h)	1032	1142	1121			
SWNTs-C_3H_6[31]	1101	1251	1215	1146	1231	1339
SWNTs-C_3H_6 (350 °C)	1105	1249	1204		1225	1338
SWNTs-C_3H_6 (400 °C)	1105	1252	1204	1249	1225	1334
					1266	

300 °C for 6 h, (8,4) SWNTs-$C_3H_4Me_2$ exhibited only the E_{11} PL peak. The emergence of new PL at red-shifted wavelengths and the increase in E_{11} PL intensity indicate competing rearrangement and elimination reactions. The results indicate that adducts of SWNTs with smaller diameter are thermally stable towards elimination, and the rearrangement reaction has the effect of shifting the PL peak to longer wavelengths.

In contrast, the separated (6,4), (8,3), and (7,5) SWNTs-$C_3H_4Me_2$, (mod(n-m, 3) = 2), exhibited new PL peaks at 1192, 1251, and 1310 nm, respectively, without thermal treatment, in addition to the PL peaks observed in SWNTs-C_3H_6 (Fig. 2a, d, and e). Relatedly, the chirality-selective emergence of NIR PL was reported to occur in the hydrobutylation of SWNTs.[25] Hydrobutylated (7,3) and (6,5) SWNTs (^{n}Bu-SWNTs-H) exhibited two new PL peaks, whereas ^{n}Bu-(6,4), (8,3), and (7,5) SWNTs-H exhibited one new PL peak, respectively. Diameter-selective increases in the E_{11} PL intensities were also observed after thermal treatment in (6,4), (8,3), and (7,5) SWNTs-$C_3H_4Me_2$. In

addition, (6,4) SWNTs-$C_3H_4Me_2$ (400 °C, 6 h) exhibited a new PL peak at 1032 nm, indicating a change in binding configuration (Fig. 2a). The change in PL wavelength selectivity and promotion of the elimination and rearrangement reactions in SWNTs-$C_3H_4Me_2$ may be attributed to the increased steric repulsion between SWNTs and addenda, and the higher stability of the SWNTs-$C_3H_4Me_2$ radical, the plausible intermediate in the reactions, compared to that of the SWNTs-C_3H_6 radical.

Fig. 3 depicts the emission energy difference (ΔPL) between functionalized and pristine SWNTs plotted as a function of the squared diameter of SWNTs. Two PL peaks observed in SWNTs-$C_3H_4Me_2$ before and after thermal treatment showed similar diameter dependence to the reported results of arylated and alkylated SWNTs,[22,30] with ΔPL values decreasing as SWNT diameters increase (Fig. 3. Black and red lines). The similar ΔPL trends for SWNTs-C_3H_6 and SWNTs-$C_3H_4Me_2$ suggest identical binding configurations for each (Fig. 3. Black and green lines). ΔPL values for (6,4) and (8,3) SWNTs-$C_3H_4Me_2$ and that after thermal treatment with the higher energy region, respectively, tended to be larger than those of others. The larger ΔPL value for the (8,3) SWNT adduct compared to those of other chiral SWNT adducts is consistent with previous reports on arylated SWNTs.[30]

As shown in Fig. 4, the 1,2-isomers are distinguished by the binding configuration of the two carbon atoms relative to the axis of SWNTs as L_{++}, L_{+}, and L_{-}, according to a pioneering report by He *et al.*[16] Previously, we calculated the relative energy and transition energy of the model compounds of (6,5) SWNTs-$C_3H_4Me_2$ isomers using density functional theory (DFT) at the level of B3LYP[32]/6-31G*[33] and time dependent (TD) DFT at the level of B3LYP/3-21G.[19,34] The wavelength shift after the thermal treatment may be attributed to the formation of 1,2-L_{++} (6,5) SWNTs-$C_3H_4Me_2$ as a kinetically preferred isomer during the functionalization reaction, while the 1,2-L_{+} (6,5) SWNTs-$C_3H_4Me_2$ is formed as the thermodynamically favored product after the thermal treatment.[31] The higher spin density at 1,2-L_{++} carbon atom in the butylated SWNTs radical supported the hypothesis that the 1,2-L_{++} adduct is the kinetically preferred product.[31]

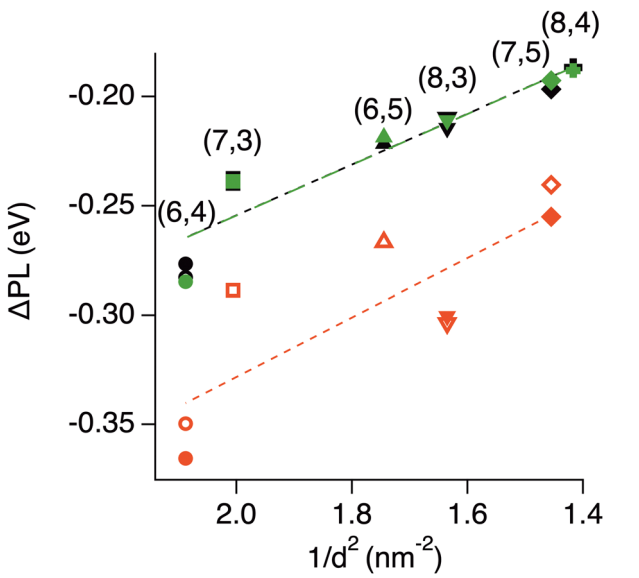

Fig. 3 Emission energy difference (ΔPL) between the functionalized and non-functionalized SWNTs as a function of the squared diameter of SWNTs.[26] SWNTs-C_3H_6 (green mark). SWNTs-$C_3H_4Me_2$ (filled black and red mark). SWNTs-$C_3H_4Me_2$ (300 °C, 6 h) (opened black and red mark). Black and red lines exhibit the linear fitting of ΔPL values for the PL peaks observed with the lower (black mark) and higher energy regions (red mark), respectively.

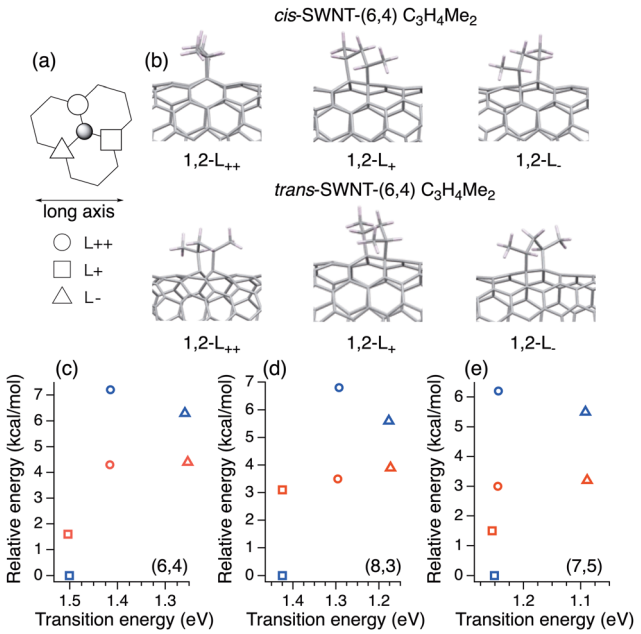

Fig. 4 (a) Three different binding configuration, marked as (○): L++, (□): L+, and (△): L−, relative to the central addition site (gray circle). (b) Optimized partial structures of (6,4) SWNT-$C_3H_4Me_2$ isomers. Calculated transition energies (eV) and relative energies (kcal mol^{-1}) of model compounds of (b) (6,4), (c) (8,3), and (d) (7,5) SWNT-$C_3H_4Me_2$ isomers. Blue: *trans*-isomer. Red: *cis*-isomer.

In this work, we evaluated the stability and transition energy of model compounds of three 1,2-addition isomers of (6,4), (8,3), and (7,5) *trans*- and *cis*-SWNT-$C_3H_4Me_2$ to consider their plausible binding configurations (Fig. S24, S25 and Table S1, ESI†).[35] As shown in Fig. 4, similar to previous findings on (6,5) SWNT-$C_3H_4Me_2$,[19] the geometric isomerism of the methyl groups has a large effect on adduct thermodynamic stability and a small effect on transition energy. In all chiral SWNTs, 1,2-L_{+}-*trans*-SWNT-$C_3H_4Me_2$ is the most stable adduct with the highest transition energy. The 1,2-L_{++}-*trans*-isomer is the most unstable adduct with an intermediate transition energy compared to those of the 1,2-L_{+} and 1,2-L_{-} isomers. Assuming that 1,2-L_{++} *trans*-SWNT-$C_3H_4Me_2$ is kinetically formed by the addition reaction, the PL peak shift in (7,3) and (6,5) SWNTs-$C_3H_4Me_2$ (mod(n-m,3) = 1) in red-shifted region can be explained by the thermodynamic rearrangement from the 1,2-L_{++} isomer to 1,2-L_{+}.[19] The two PL peaks exhibited by (6,4), (8,3), and (7,5) SWNTs-$C_3H_4Me_2$ may be attributed to the 1,2-L_{++} and 1,2-L_{-} isomers, which show small energy differences. Relatedly, it was reported that the spin densities at the 1,2-L_{-} carbon

atoms of butylated (6,4), (8,3), and (7,5) SWNT radicals (0.1571, 0.1564, 0.1568) were slightly higher than those at the 1,2-L_+ carbon atoms of butylated (7,3), (6,5), and (8,4) SWNT radicals (0.1440, 0.1479, 0.1506), respectively.[30] However, further investigation is required to clarify the chiral index dependency. In addition, (6,4) SWNTs-$C_3H_4Me_2$ exhibited new PL peak at 1032 nm with an increase of the intrinsic E_{11} PL; this can be explained by the thermodynamic rearrangement to the most stable 1,2-L_+ isomer. The PL wavelength is similar to that of a previously reported PL peak at 1015 nm in ^{n}Bu-(6,4) SWNTs-H, for which the 1,2-L_+ binding configuration was proposed.[26] The thermal treatment of alkylated SWNTs[11,36] and photoirradiation of phenylated SWNTs[37] having two PL peaks emerged after functionalization was reported to increase the short- to long-wavelength PL intensity ratio. In contrast, a key factor in the thermal PL redshift is that cycloaddition affords kinetically controlled products, and the methyl groups promote the rearrangement reaction.

In conclusion, we demonstrate chirality- and diameter-dependent thermal rearrangement of addenda on SWNTs prompted by methyl groups competing with the elimination reaction. Functionalized SWNTs underwent chiral separation before and after thermal treatment and the optical properties of the products were analyzed. The results clarified that elimination reactions occur predominantly in adducts of large-diameter SWNTs, whereas competitive rearrangement reactions occur in smaller diameter (7,3) and (6,5) SWNTs-$C_3H_4Me_2$, resulting in redshifts in the PL wavelength. Conversely, without thermal treatment, (6,4), (8,3), and (7,5) SWNTs-$C_3H_4Me_2$ exhibited two PL peaks due to the substitution of methyl groups. The shift in PL wavelength beyond the optical communication wavelength range and the selectivity afforded by the substituent effect of methyl groups and thermal treatment provide a new perspective on the design and structural analysis of functionalized SWNTs.

This work was supported by JSPS KAKENHI Grant-in-Aid for Scientific Research (B) (21H01759, 20H02210, 20H02718, 17H02735) and Transformative Research Areas (A) (22H05133). The computations were partially performed in the Research Center for Computational Science, Okazaki, Japan (Project: 22-IMS-C185).

Conflicts of interest

There are no conflicts to declare.

Notes and references

1 S. Iijima and T. Ichihashi, *Nature*, 1993, **363**, 603–605.
2 D. S. Bethune, C. H. Kiang, M. S. de Vries, G. Gorman, R. Savoy, J. Vazquez and R. Beyers, *Nature*, 1993, **363**, 605–607.
3 D. Tasis, N. Tagmatarchis, A. Bianco and M. Prato, *Chem. Rev.*, 2006, **106**, 1105–1136.
4 N. Karousis, N. Tagmatarchis and D. Tasis, *Chem. Rev.*, 2010, **110**, 5366–5397.
5 S. Banerjee and S. S. Wong, *Nano Lett.*, 2004, **4**, 1445–1450.
6 B. Gebhardt, R. Graupner, F. Hauke and A. Hirsch, *Eur. J. Org. Chem.*, 2010, 1494–1501.
7 D. Wunderlich, F. Hauke and A. Hirsch, *Chem. – Eur. J.*, 2008, **14**, 1607–1614.
8 H. Hu, B. Zhao, M. A. Hamon, K. Kamaras, M. E. Itkis and R. C. Haddon, *J. Am. Chem. Soc.*, 2003, **125**, 14893–14900.
9 E. T. Mickelson, C. B. Huffman, A. G. Rinzler, R. E. Smalley, R. H. Hauge and J. L. Margrave, *Chem. Phys. Lett.*, 1998, **296**, 188–194.
10 S. Ghosh, F. Wei, S. M. Bachilo, R. H. Hauge, W. E. Billups and R. B. Weisman, *ACS Nano*, 2015, **9**, 6324–6332.
11 Y. Maeda, Y. Takehana, J. S. Dang, M. Suzuki, M. Yamada and S. Nagase, *Chem. – Eur. J.*, 2017, **23**, 1789–1794.
12 A. H. Brozena, M. Kim, L. R. Powell and Y. Wang, *Nat. Rev. Chem.*, 2019, **3**, 375–392.
13 D. Janas, *Mater. Horiz.*, 2020, **7**, 2860–2881.
14 J. Ackermann, J. T. Metternich, S. Herbertz and S. Kruss, *Angew. Chem., Int. Ed.*, 2022, **61**, e202112372.
15 X. Ma, L. Adamska, H. Yamaguchi, S. E. Yalcin, S. Tretiak, S. K. Doorn and H. Htoon, *ACS Nano*, 2014, **8**, 10782–10789.
16 X. He, B. J. Gifford, N. F. Hartmann, R. Ihly, X. Ma, S. V. Kilina, Y. Luo, K. Shayan, S. Strauf, J. L. Blackburn, S. Tretiak, S. K. Doorn and H. Htoon, *ACS Nano*, 2017, **11**, 10785–10796.
17 P. Zhao, Y. Maeda and M. Ehara, *J. Phys. Chem. C*, 2019, **123**, 18629–18637.
18 Y. Maeda, K. Kuroda, H. Tambo, H. Murakoshi, Y. Konno, M. Yamada, P. Zhao, X. Zhao, S. Nagase and M. Ehara, *RSC Adv.*, 2019, **9**, 13998–14003.
19 Y. Maeda, H. Murakoshi, H. Tambo, P. Zhao, K. Kuroda, M. Yamada, X. Zhao, S. Nagase and M. Ehara, *Chem. Commun.*, 2019, **55**, 13757–13760.
20 Y. Zhang, N. Valley, A. H. Brozena, Y. Piao, X. Song, G. C. Schatz and Y. Wang, *J. Phys. Chem. Lett.*, 2013, **4**, 826–830.
21 Y. Maeda, S. Minami, Y. Takehana, J. S. Dang, S. Aota, K. Matsuda, Y. Miyauchi, M. Yamada, M. Suzuki, R. S. Zhao, X. Zhao and S. Nagase, *Nanoscale*, 2016, **8**, 16916–16921.
22 H. Kwon, A. Furmanchuk, M. Kim, B. Meany, Y. Guo, G. C. Schatz and Y. Wang, *J. Am. Chem. Soc.*, 2016, **138**, 6878–6885.
23 X. He, N. F. Hartmann, X. Ma, Y. Kim, R. Ihly, J. L. Blackburn, W. Gao, J. Kono, Y. Yomogida, A. Hirano, T. Tanaka, H. Kataura, H. Htoon and S. K. Doorn, *Nat. Photon.*, 2017, **11**, 577–582.
24 D. Yang, L. Li, X. Wei, Y. Wang, W. Zhou, H. Kataura, S. Xie and H. Liu, *Sci. Adv.*, 2021, **7**, eabe0084.
25 Y. Maeda, Y. Konno and M. Yamada, *J. Phys. Chem. C*, 2020, **124**, 21886–21894.
26 Y. Maeda, R. Morooka, P. Zhao, D. Uchida, Y. Konno, M. Yamada and M. Ehara, *J. Phys. Chem. C*, 2023, **127**, 2360–2370.
27 S. M. Bachilo, M. S. Strano, C. Kittrell, R. H. Hauge, R. E. Smalley and R. B. Weisman, *Science*, 2002, **298**, 2361–2366.
28 X. Wei, T. Tanaka, Y. Yomogida, N. Sato, R. Saito and H. Kataura, *Nat. Commun.*, 2016, **7**, 12899.
29 X. Wei, T. Tanaka, T. Hirakawa, Y. Yomogida and H. Kataura, *J. Am. Chem. Soc.*, 2017, **139**, 16068–16071.
30 Y. Piao, B. Meany, L. R. Powell, N. Valley, H. Kwon, G. C. Schatz and Y. Wang, *Nat. Chem.*, 2013, **5**, 840–845.
31 Y. Konno, R. Morooka, T. Morishita, P. Zhao, N. Miyasaka, K. Ono, A. Noda, D. Uchida, R. Iwasaki, M. Yamada, M. Ehara and Y. Maeda, *Chem. – Eur. J.*, 2023, **29**, e202300766.
32 A. D. Becke, *J. Chem. Phys.*, 1993, **98**, 5648–5652.
33 R. Ditchfield, W. J. Hehre and J. A. Pople, *J. Chem. Phys.*, 1971, **54**, 724–728.
34 J. S. Binkley, J. A. Pople and W. J. Hehre, *J. Am. Chem. Soc.*, 1980, **102**, 939–947.
35 M. J. Frisch, G. W. Trucks, H. B. Schlegel, M. A. Robb, J. R. Cheeseman, G. Scalmani, V. Barone, B. Mennucci, G. A. Petersson, *et al.*, *Gaussian 09, Revision E.01*, Gaussian, Inc., Wallingford CT, 2013.
36 Y. Maeda, Y. Konno, M. Yamada, P. Zhao, X. Zhao, M. Ehara and S. Nagase, *Nanoscale*, 2018, **10**, 23012–23017.
37 H. Qu, X. Wu, J. Fortner, M. Kim, P. Wang and Y. Wang, *ACS Nano*, 2022, **16**, 2077–2087.